Microwave multiphoton transitions between Rydberg states of potassium

R. C. Stoneman, D. S. Thomson, and T. F. Gallagher
Department of Physics, University of Virginia, Charlottesville, Virginia 22901
(Received 31 August 1987)

Observations are reported of complete sequences of N-photon resonant microwave transitions, in potassium, from the $(n+2)s$ state to the lowest energy state of the linear Stark manifold of principal quantum number n. The number N of photons absorbed ranges from 1 to as high as 30, and n is in the range from 16 to 19. A sequence is observed by scanning the static electric field, starting at the field at which the levels undergo an avoided crossing, until zero field is reached. The maximum number of photons absorbed is observed to be proportional to the microwave field amplitude, with an offset of two photons at zero field. Dynamic Stark shifts of the levels are observed to be proportional to the microwave power. The n dependence and absolute size of the shift are in agreement with Floquet calculations. The relation between the N-photon resonances and microwave ionization is discussed. In particular, resonances in microwave ionization spectra are seen to be due to dynamic-Stark-shifted multiphoton transitions.

I. INTRODUCTION

Electric field ionization has proved to be a valuable technique for selectively detecting highly excited, or Rydberg, atoms.[1-6] A variety of experiments has shown that, for atoms other than hydrogen, ionization occurs at the saddle point of the potential surface of the combined Coulomb and static electric fields. The field (in atomic units) at which this classical ionization takes place is given by $1/16n^4$, where n is the principal quantum number.

For microwave fields, however, ionization has been observed to occur at lower field amplitudes than for static or slowly rising ($\sim 1\ \mu$s) electric fields. In Na and He, for example, the threshold field for microwave ionization[7-9] is observed to vary as $1/n^5$. Microwave ionization therefore requires another mechanism in addition to the classical $1/n^4$ field ionization. This mechanism is provided by the avoided level crossing of the highest-energy linear Stark state of principal quantum number n with the lowest-energy Stark state of principal quantum number $n+1$. This crossing occurs at the static field of $1/3n^5$. If the microwave field amplitude reaches this avoided crossing, and the microwave frequency is comparable to the minimum separation of the avoiding levels, the atom can undergo a Landau-Zener transition at the avoided crossing from the n Stark manifold to the $n+1$ manifold. The transitions to still higher Stark manifolds then follow, since the higher manifold-to-manifold crossings occur at lower fields, until finally a state is reached which can be classically ionized by the microwave field. In any case, the $n \rightarrow n+1$ Landau-Zener transition is the rate-limiting step in the ionization process. This interpretation of the $1/3n^5$ ionization is supported by several observations. First, the presence of a static field F_s depresses the required microwave field by F_s, implying that the total field must always reach the avoided crossing, as expected for a Landau-Zener transition. Second, the analogous transition of a state of nonzero quantum defect δ to the adjacent Stark manifold is observed to occur at a field of $2\delta/3n^5$, where δ/n^3 is the energy separation from the nearest hydrogenic level.

The Landau-Zener theory strictly applies to the case where the electric field varies through the avoided crossing linearly in time (for t ranging from $-\infty$ to $+\infty$). Rubbmark *et al.*[10] have generalized this notion and have studied the avoided-crossing traversal problem for experimentally realizable electric field pulses. They have calculated the probability of diabatic traversal of the avoided crossing by numerically integrating the Schrödinger equation for two coupled levels, each with linear Stark shifts away from the avoided crossing, for various types of pulses. Their calculations show resonant behavior when the field pulse has spectral content near the minimum separation of the avoiding levels. Pillet *et al.*[9] have applied their calculational technique to the $1/3n^5$ transitions of microwave ionization. Specifically, they calculated the probability of making a transition from the highest-lying n Stark state to the lowest-lying $n+1$ Stark state with one half-cycle of the microwave field. Only a half-cycle was used since transitions between states of the same n were observed to be rapid and were assumed to be so much more rapid than the Δn transition that coherence over many cycles was not possible. These calculations showed that the probability of making the Δn transition was high if the microwave field very nearly reached the crossing and the microwave frequency was approximately equal to the size of the avoided crossing.

We have extended the Landau-Zener calculations of Pillet *et al.*[9] to the case in which there are many cycles of the microwave field and a static field is present as well. When there are many coherent cycles of the microwave field, the transition amplitudes for successive cycles can add constructively or destructively, and as a result resonances occur in the transition probabilities. The resonances occur when the separation between the levels, which is determined mainly by the Stark shift of the static field, but has a small contribution from the microwave field, is equal to an integer times the microwave frequen-

cy. A particular resonance has appreciable strength if the peak electric field, i.e., the sum of the static field and amplitude of the oscillating field, approaches the avoided crossing.

With this connection between the Landau-Zener effect and multiphoton resonances in mind, it is reasonable to expect that an experimental study of these Landau-Zener, or multiphoton, transitions will be most instructive. In particular, it will provide valuable information concerning the rate-limiting step of microwave ionization without all the complications of the actual ionization. Here we expand on our previous report[11] on observations of resonant microwave multiphoton transitions between Rydberg states of potassium. Specifically, we have observed resonant transitions from the $(n+2)s$ state to a member of the linear Stark manifold with principal quantum number n and have measured the threshold microwave field for this process in order to make explicit the connection with the microwave ionization experiments, for n in the range 16–19. The relevant potassium energy levels are shown in Fig. 1 for $n=17$. The states with $l>2$ are nearly degenerate in zero static field (for a given n), and therefore have approximately linear Stark shifts. We will use the notation (n,n_1) for the manifold state which connects adiabatically to the zero-field state with $l=n_1$. The s state has quantum defect $\delta_s=2.18$, placing the $19s$ state approximately 8 cm^{-1} below the $n=17$ manifold. The manifold states contain very little p character, as can be seen from the behavior of the $19p$ state in Fig. 1. As a result the s state has relatively little Stark shift and small avoided crossings with the lowest linear Stark states.

The observations of microwave resonances were concentrated primarily on transitions to the lowest manifold level. In this case the one-photon resonance is observed at a field just below the first s-state avoided crossing, and resonances involving progressively more photons are found at progressively lower values of the static field. In Fig. 1 the N-photon transitions are indicated by the vertical arrows for $N=5$ and 10 (for 9.278 GHz photons). For $n=17$ the manifold to s-state energy separation in zero static field is such that, for 9.278 GHz microwave photons, transitions for N as large as 26 can be observed before the static field reaches zero. The resonances occur at the static field interval $\hbar\omega/S$, where ω is the microwave angular frequency and $S=dW/dF$ is the differential Stark shift of the levels involved, where F is the static electric field and $W=$(energy of manifold state)$-$(energy of s state). Therefore the spacing is smallest for the transitions to the extreme members of the manifold.

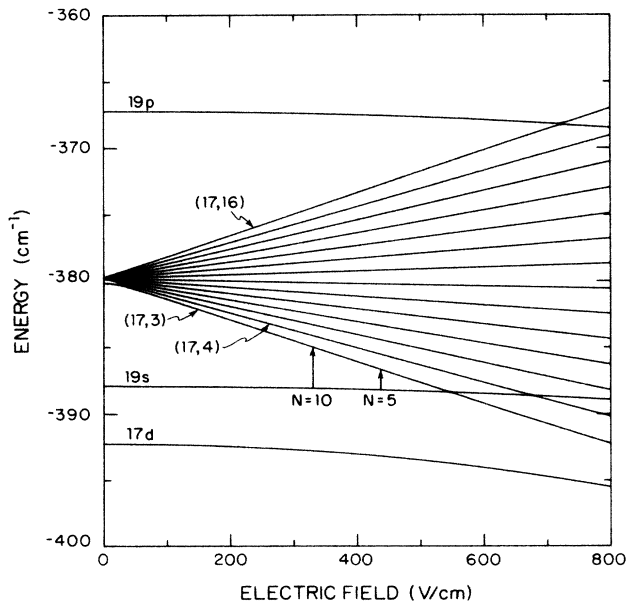

FIG. 1. Stark energy levels of potassium in the vicinity of $n=17$. The notation (n,n_1) indicates the manifold state which connects adiabatically to the zero-field state with $l=n_1$. The N-photon transitions are indicated for $N=5$ and 10 (for 9.278-GHz photons).

In Sec. II we describe the experimental approach. In Sec. III we present our observations, beginning with the threshold microwave fields required to drive the $(n+2)s$-to-n manifold transitions. Unlike the microwave ionization thresholds, which exhibit a smooth $1/3n^5$ dependence, these thresholds do not exhibit a smooth $1/3n^5$ behavior, and in addition exhibit structure. Observations of microwave multiphoton resonances, including a careful investigation of the transition rates and dynamic Stark shifts produced by the microwave field, allow us to account for the irregularities in the microwave threshold fields for the $(n+2)s$-to-n manifold transitions. The observed transition rates and dynamic Stark shifts are compared to theoretical calculations based on the Landau-Zener theory and on a Floquet approach. Finally, in Sec. IV the Floquet method is used to calculate the dynamic Stark structure, which is compared to the observed dynamic Stark shifts.

II. EXPERIMENTAL APPROACH

A schematic diagram of the experimental apparatus[11] is shown in Fig. 2. A beam of ground-state potassium atoms enters a microwave cavity through a small hole in the cavity sidewall. The potassium atoms are stepwise excited to the Rydberg s state by two pulsed dye lasers. The first, with wavelength 770 nm, excites the $4s$ ground state to the $4p_{1/2}$ state, and the second, with wavelength $\sim$460 nm, drives the $4p_{1/2}$ state to the desired $(n+2)s$ state. The laser beams propagate antiparallel to the atomic beam and enter the cavity through the opposite sidewall. Following the laser pulses a 0.3-μs microwave

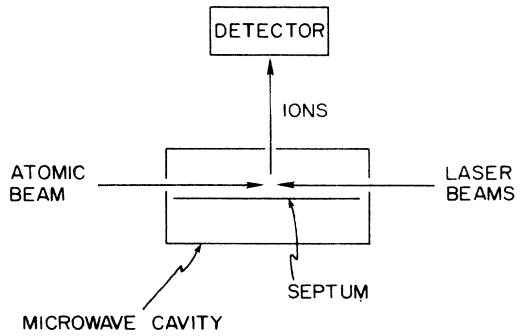

FIG. 2. Schematic diagram of the experimental apparatus.

pulse at 9.278 or 10.353 GHz drives the multiphoton transitions. Then a high-voltage pulse is applied to a copper septum in the cavity, producing an electric field which ionizes the excited atoms. The resulting ions leave the cavity through a small hole in the center of its top wall and are detected by a microchannel plate detector. This signal is amplified and sent to an integrator which is gated to accept only the signal from the atoms which have been excited to the manifold states. The integrator output is collected and averaged by a microcomputer. The signal from the microwave-excited atoms occurs earlier than the signal from the s state, since the manifold levels are ionized at a lower electric field and therefore earlier in the field ionization pulse. In general the manifold levels with higher n_1 are ionized earlier and the signals arising from the various manifold levels can usually be time resolved. The amplitude and slew rate of the ionization pulse are adjusted to optimize this resolution.

The microwave cavity is a 20.32-cm-long piece of X-band rectangular waveguide which is closed at both ends.[9] The septum is located just below the laser- and atomic-beam entrance holes. The cavity is operated in the TE_{10n} mode, where n is odd, producing an electric field antinode (with respect to the directions parallel to the septum) at the center of the cavity. In this mode the microwave and static fields are parallel. The $n=9$ and 11 modes, with resonant frequencies 9.278 and 10.353 GHz, respectively, have been used in the measurements described here. The cavity is excited by a probe located a quarter wavelength from one end. The microwave source is an Avantek model 7872 yttrium-iron garnet-tuned oscillator, amplified by a Litton model 624 pulsed-traveling-wave tube amplifier. A small portion of the oscillator output is coupled out to a counter, allowing us to monitor the frequency. A variable crossed-vane attenuator placed between the oscillator and amplifier provides continuous variation of the microwave power. A circulator between the amplifier and cavity allows us to monitor the power reflected from the cavity. The oscillator frequency was adjusted to maintain the reflected power at a minimum. The cavity has a measured Q of 1100, producing an electric field of 190 V/cm with 1 W of power input.[12] The microwave power was calibrated with a Hewlett Packard 432A power meter. We estimate an uncertainty of 10% in the field calibration, due primarily to geometrical factors. Contributing to this is uncertainty in the location of the interaction region, defined by the overlap of the atomic and laser beams with the ion extraction hole, relative to the cavity antinode. The conversion from microwave power to electric field strength is also dependent on the cavity geometry.

Two types of data are reported here, multiphoton resonance spectra and threshold field scans. The multiphoton resonance spectra are obtained by sweeping the static field from the s-state crossing field to zero field, for a fixed microwave-field amplitude. The static field is produced by applying a dc voltage to the septum and is swept repetitively by a computer. The separation between the septum and top wall of the cavity is 0.4657(2) cm. This dimension is inferred from the known s-state anticrossing fields.[13] To be precise, we calculated the field of the one-photon resonance using the known s anticrossing fields and the static Stark shifts which are calculated using the method described in Sec. III D. The implied assumption that the dynamic Stark shift due to the microwave field is negligible at the field strength required for a one-photon transition will later be shown to be valid. The static field homogeneity is approximately 0.5%.

Also observed are threshold field scans, which are analogous to microwave ionization thresholds. In these the static field is zero, while the microwave field amplitude is swept from zero to a value beyond the s-state crossing field. These spectra are obtained by mechanically scanning the attenuator with a geared synchronous motor. These types of data do not benefit from the long-term averaging used for the multiphoton resonance spectrum, since successive sweeps of the attenuator are difficult to align.

III. OBSERVATIONS AND INTERPRETATION

A. Microwave threshold spectra

In Fig. 3 we show the observed probability for making the $18s$-to-$n=16$ manifold transition as the 9.278-GHz microwave field is varied while the static field is zero. The laser populates the $18s$ state and the $n=16$ manifold states are detected. These data are similar to the microwave ionization data, which are also obtained by varying the microwave field. In Fig. 3, however, the signal from the $n=16$ manifold is detected using selective pulsed field ionization, while no such field is used in microwave ionization. The two types of data are similar, however, in displaying a smooth threshold as the microwave field is increased. In the $18s$-to-$n=16$ transition spectrum the smooth threshold occurs at the crossing field of the $18s$ and (16,3) states, while the threshold in the $18s$ microwave ionization spectrum occurs at the

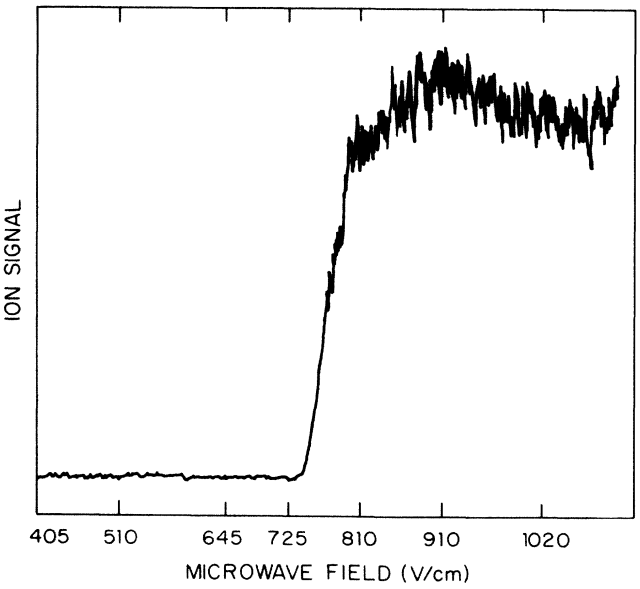

FIG. 3. Microwave threshold spectrum for transitions from the $18s$ state to the $n=16$ Stark manifold.

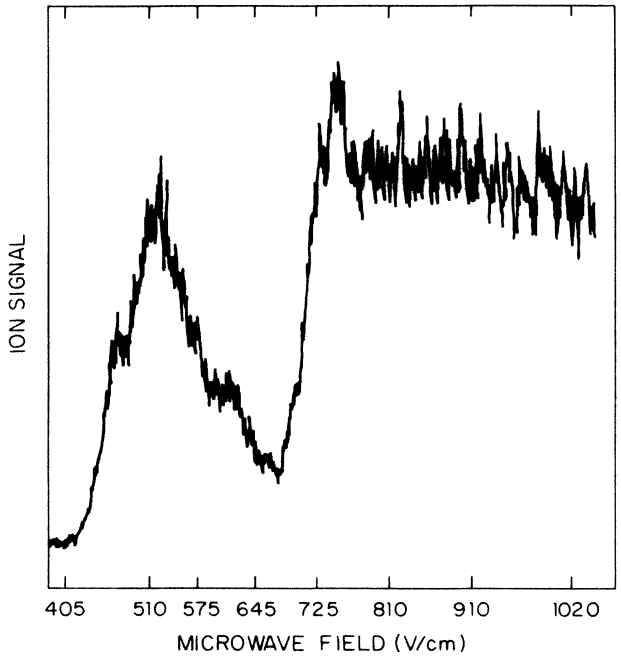

FIG. 4. Microwave threshold spectrum for transitions from the 19s state to the $n=17$ Stark manifold. The resonance near 510 V/cm corresponds to the absorption of 27 microwave photons.

crossing of the highest-energy $n=16$ state with the lowest-energy $n=17$ state.

The 9.278 GHz spectrum for transitions from the 19s state to the $n=17$ manifold is shown in Fig. 4. This spectrum, with an obvious structure at low field in addition to the smooth threshold, is qualitatively different from the 18s spectrum. As we shall show in an explicit fashion, the structure at low field is due to a multiphoton transition which is brought into resonance by the dynamic Stark shift of a 515-V/cm microwave field. Data analogous to those shown in Figs. 3 and 4 were taken for several states at the microwave frequency of 9.278 GHz. In Table I we list the observed threshold and resonance fields for transitions from the $(n+2)s$ states, for n in the range 16–21. As a threshold we have taken the point where the signal has reached 50% of its final value. In Table I we have also listed the fields of the avoided crossings of the $(n+2)s$ states with the lowest Stark states $(n,3)$. It is evident that the threshold fields do not exhibit a smooth n dependence, as do the microwave ionization threshold fields, but rather vary from near the crossing field to 150 V/cm above the crossing field. As we shall see, this can also be understood in terms of multiphoton resonances.

TABLE I. Observed threshold and resonance fields for the $F_s=0$, $(n+2)s$-to-n manifold transitions and corresponding avoided crossing fields.

$(n+2)s$ state	Observed threshold field (V/cm)	Observed resonance field (V/cm)	Avoided crossing field[a] (V/cm)
18s	775		753
19s	695	515	546
20s	405		404
21s	455		304
22s	295		233
23s	285		180

[a]From Ref. 21.

B. Multiphoton resonance spectra

Most of our efforts were focused on the study of resonant transitions. A typical example of the multiphoton resonance spectrum is shown in Fig. 5 for transitions from the 19s state. Similar spectra were taken for 18s, 20s, and 21s. Each trace is taken at a particular microwave field amplitude, which is indicated at the left of the trace. A large majority of the strongest resonances are spaced evenly with respect to the static field. These resonances represent N-photon transitions from the 19s state to the (17,3) manifold state. The number N of photons absorbed is indicated at the top of the figure. The remaining resonances seen in the figure represent transitions to the other manifold states, primarily the (17,4) state. For a given microwave field amplitude, resonances are not observed for static fields below those shown in the traces of Fig. 5. Therefore it is clear that progressively higher microwave fields are required for the resonances having higher N, which occur at progressively lower static fields. In fact, the figure suggests that a particular resonance becomes observable when the total field, static plus microwave, exceeds some constant value. It should be noted that this observation is consistent with the previously mentioned Landau-Zener picture, in which transitions occur when the total field approaches the avoided-crossing field. For the multiphoton resonance spectrum, the relevant crossing is that of the s state with the manifold state.

In order to make this point in a more quantitative fashion, in Fig. 6 the microwave field required to observe a particular 19s-to-(17,3) multiphoton resonance is plotted versus the number of photons absorbed. The fractional part of the "number of photons" in Fig. 6 is defined to be the strength of the weakest observable transition as a fraction of saturation. For example, in Fig. 5(a) a microwave field of 68 V/cm allows us to observe 6.2 photons. This threshold for observation of a particular resonance is somewhat uncertain since it depends on the nonlinearity of saturation, the detection sensitivity of the apparatus, and the broadening effects due to electric field inhomogeneity. In spite of these limitations, however, Fig. 6 clearly shows that the number of photons absorbed increases linearly with the microwave field. Specifically, the line in Fig. 6 is a linear least-squares fit to the data points. The linearity of the data is consistent with the Landau-Zener picture, since the number of photons absorbed is proportional to the difference of the static field and the crossing field. It is also important to note that there is approximately a two-photon offset in the fit of Fig. 6. That is, the one- and two-photon transitions are driven with very small microwave fields, while higher

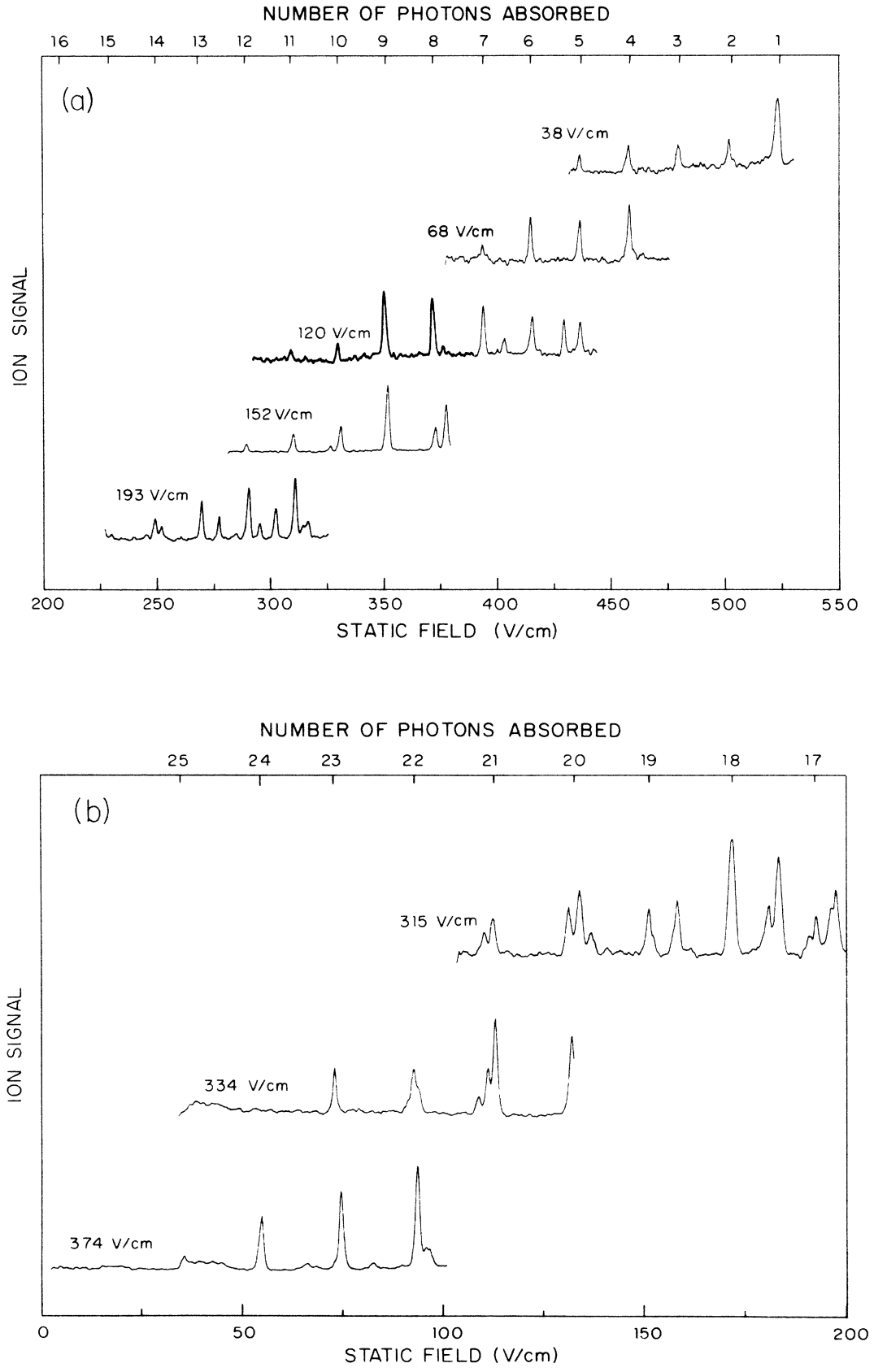

FIG. 5. Multiphoton resonance spectrum for transitions from the 19*s* state to the $n = 17$ Stark manifold. Each trace is taken at a fixed microwave field, indicated at the left of the trace. The number of photons absorbed, for transitions to the (17,3) level, is shown at the top of the figure.

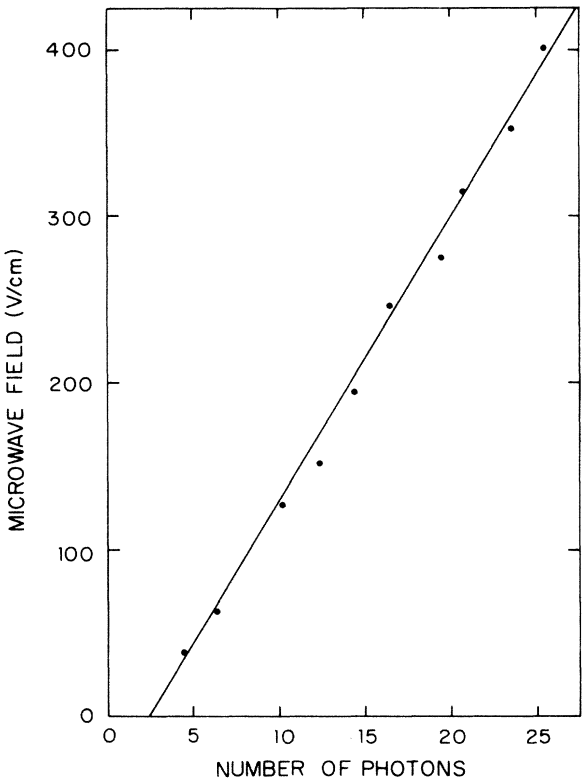

FIG. 6. Microwave field required to observe the 19s-to-(17,4) multiphoton transition vs the number of photons absorbed. The line is a least-squares fit to the data points, demonstrating that the total field, static plus microwave, required to drive the multiphoton transitions is constant. Note the two-photon offset at zero field.

N-photon transitions require a constant additional microwave field for each additional photon. We shall see that these features emerge quite naturally from a dressed atom description of the process.

In describing Fig. 5 we noted that nearly all the observed transitions which occurred at regular static field intervals were 19s-to-(17,3) transitions and that transitions not fitting this pattern were transitions to higher energy $(17,n_1)$ Stark states, with $n_1 > 3$. This is shown explicitly in Fig. 7, where the strongest peaks of the 193-V/cm (microwave field) trace are identified, using the notation $[n_1,N]$. Two points are worth noting. The transitions to higher-energy Stark levels occur at larger static field intervals due to the smaller Stark shifts of these levels and the transitions become observable when the total field, static plus microwave, reaches the crossing of that Stark level with the s state.

C. Connection between the photon and field points of view

These observations can be explained in greater depth if we examine the connection between the photon and field points of view as it relates to transitions at an avoided crossing. For simplicity, we will consider a two-level system which approximates the levels which undergo the avoided crossing, the $(n+2)s$ and $(n_1,3)$ states, as shown

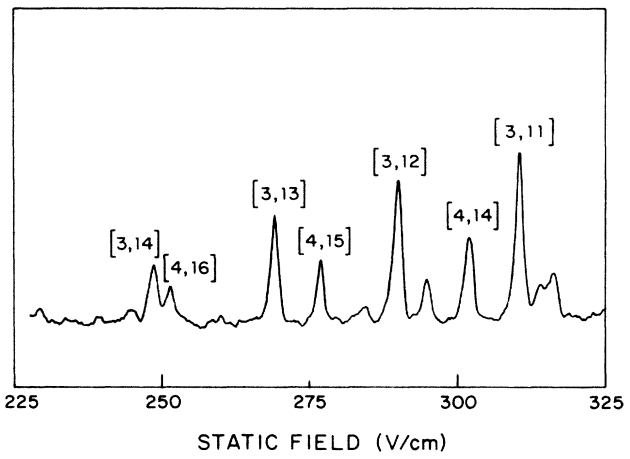

FIG. 7. Identification of the multiphoton resonant transitions from the 19s state at the 193-V/cm microwave field. The peaks are labeled $[n_1,N]$, where N is the number of photons absorbed. Note that the transitions to the lowest Stark manifold state $n_1 = 3$ are more closely spaced than those to the state $n_1 = 4$, due to the larger Stark shift for $n_1 = 3$.

in Fig. 8. The s state, $|2\rangle$ in Fig. 8, is assumed to have no Stark shift, while the manifold state, $|1\rangle$ in Fig. 8, has a Stark shift $-kF$, where F is the electric field. The levels cross at the field F_c when the coupling between them is ignored. When the coupling $b = \langle 1|V|2\rangle$ is taken into account the levels repel, producing the avoided crossing with closest approach $2b$. Our goal is to calculate the dependence on microwave field of the transition probabilities for the multiphoton resonances which occur as the static field is tuned. As an example of such a reso-

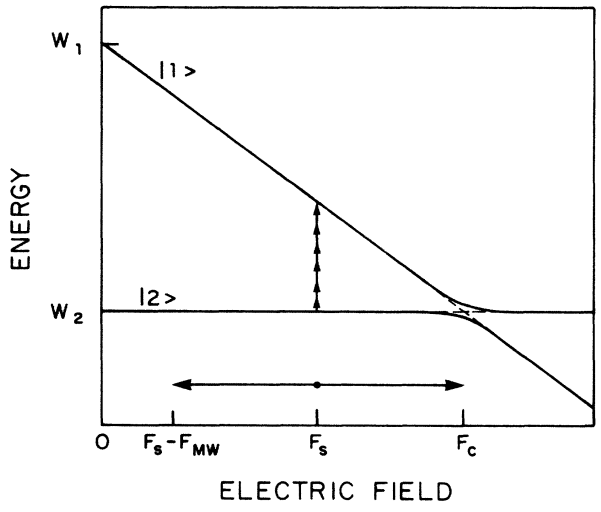

FIG. 8. Multiphoton resonant transition at an avoided crossing from the photon and field points of view. The solid curves are the avoiding levels and the dashed lines are the levels which cross when the coupling is ignored. The static field F_s gives rise to a six-photon resonant transition, indicated by the stacked arrows. The range of the electric field variation is shown for the case in which the peak field $F_s + F_{MW}$ exactly reaches the crossing field F_c. The size of the avoided crossing is exaggerated for clarity.

nance, the six-photon transition is shown in Fig. 8.

If the wave function of this two-level system is represented by $\psi = T_1(t)\,|1\rangle + T_2(t)\,|2\rangle$, then the Schrödinger equation leads to two coupled equations,

$$\begin{aligned} i\dot{T}_1 &= (W_1 - kF)T_1 + bT_2 \ , \\ i\dot{T}_2 &= bT_1 + W_2 T_2 \ , \end{aligned} \tag{1}$$

where W_1 and W_2 are the zero-field energies. If the field is static the solution is time independent and can be obtained by diagonalizing the Hamiltonian matrix, leading to the energies shown by the solid lines of Fig. 8. We are, however, interested in the case in which a microwave as well as a static field is present. In this case the electric field is given by

$$F(t) = F_s + F_{\mathrm{MW}} \cos\omega t \ , \tag{2}$$

and the solution is no longer time independent. Here F_s is the static field, F_{MW} is the microwave field amplitude, and ω is the microwave angular frequency. We wish to calculate the probability for an atom originally in state $|2\rangle$ making a transition to state $|1\rangle$. We shall use two approaches to this problem, corresponding to the photon and field points of view. From the field point of view the microwave field brings the atoms to the avoided crossing at F_c, where they undergo a Landau-Zener transition.[14,15] From the photon point of view the multiphoton transitions are treated in the Floquet, or dressed atom, approach.[16,17] The calculations must ultimately be done numerically and for this purpose we have chosen parameters appropriate to the 19*s*-to-(17,3) transition. Specifically we will use $W_1 = 220$ GHz, $W_2 = 0$, $F_c = 550$ V/cm [therefore $k = 400$ MHz/(V/cm)], and $b = 400$ MHz, and we will use 10 GHz as the microwave frequency. With these parameters the resonances occur at the static field interval of 25 V/cm.

From the field point of view the resonant transitions can be thought of as a generalization of the Landau-Zener effect. Landau and Zener treated the case where the variation of the electric field through the avoided crossing is linear with respect to time. They found that the probability for making the diabatic transition at the avoided crossing is[14,15]

$$P = \exp\left[\frac{-2\pi\omega_0^2}{(dW/dF)(dF/dt)}\right] , \tag{3}$$

where $\omega_0 = 2b$ is the separation of the levels at the avoided crossing, dW/dF is the differential slope of the levels (ignoring the coupling), and dF/dt is the rate of change of the electric field.

Rubbmark *et al.*[10] have calculated the diabatic transition probability for fields that do not vary linearly in time in traversing the avoided crossing. In particular, they have considered cases for which the electric field variation turns on slowly, passes through the crossing region, and then turns off slowly. The transition probabilities are obtained by numerically integrating the time-dependent Schrödinger equation for the two coupled levels. Through an appropriate change of variables they are able to use the Numerov integration method, which applies when the differential equation is second order, linear, and contains no first-order term. The calculations show resonant behavior when the field variation has harmonic components near ω_0.

Rubbmark *et al.* were interested in diabatic transitions induced by field pulses. That is, they considered only monotonic variation of the electric field through the avoided crossing. The Numerov method can be applied, however, to any variation of the electric field as a function of time. In particular, we will assume that the electric field has the form of Eq. (2). In Fig. 8 the range of the electric field variation is shown for the case in which the peak field $F_s + F_{\mathrm{MW}}$ exactly reaches the crossing field F_c. Resonances in the calculated transition probability begin to appear when the oscillation continues for at least a few cycles. The connection between the slowly varying field point of view, in which Landau-Zener transitions are the model, and the resonance point of view, in which multiphoton transitions are the model, therefore arises in a continuous, natural fashion.

Multiphoton resonances appear in the Numerov calculations whenever the static field is such that the separation between the levels matches an integer multiple of the microwave oscillation frequency. The static field F_s shown in Fig. 8 gives rise to a six-photon resonant transition, indicated by the stacked arrows. A resonance can be observed in one of two ways: the frequency can be swept at fixed static field or the static field can be swept at fixed frequency. As can be seen in Fig. 5, we are interested in the latter situation. Figure 9 shows a typical resonance obtained from the numerical integration technique. Specifically the six-photon resonance at 400 V/cm, which occurs 150 V/cm below the crossing field, is shown. The resonance is calculated with a microwave

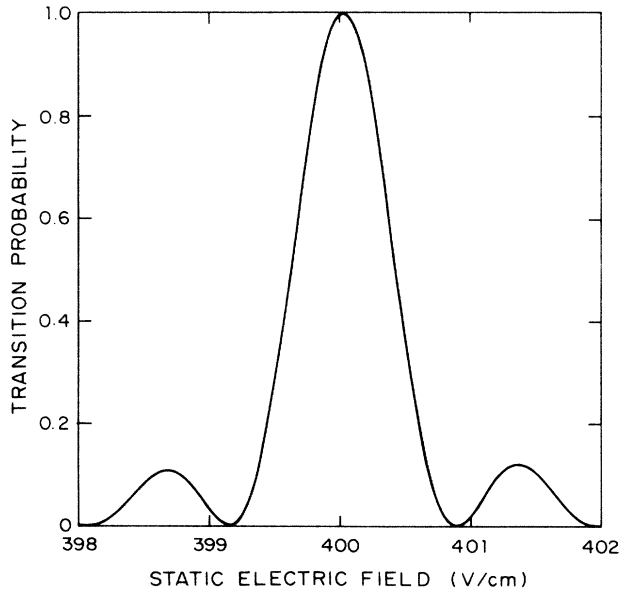

FIG. 9. Transition probability calculated by numerical integration of the two-level Schrödinger equation for the six-photon transition shown in Fig. 8. The microwave field is 150 V/cm.

field amplitude of 150 V/cm and the previously mentioned values for k, ω, and b appropriate to the 19s avoided crossing.

The line shape of the resonance shown in Fig. 9 is very similar to the Rabi resonance pattern[18] and can therefore be characterized by three parameters, the line center F_0, the full width at half maximum ΔF, and interaction time t. The field width ΔF is related to the Rabi frequency Ω by $\Delta F = 4\Omega(dW/dF)$. This parameter is of primary importance since it represents the strength of the transition. The resonance represents a six-photon transition since the line center is very close to 400 V/cm. The interaction time has been chosen to produce the "optimum perturbation"[18] ($\Omega t = \pi/2$). We determine the values of the resonance parameters by a least-squares fit of the calculated resonance to the ideal Rabi pattern. For Fig. 9 the results are $F_0 = 400.02$ V/cm, $\Delta F = 0.99$ V/cm, and $\Omega t = 0.99(\pi/2)$. The Rabi line shape provides an excellent model for the calculated resonance, but a small degree of asymmetry is evident in Fig. 9. For example, the wing at the right of the main peak is slightly larger than the left-hand wing. It is reasonable to assume that this asymmetry is minimized at optimum perturbation.

We cannot expect to observe the Rabi pattern in our experiment since it will be washed out by static and microwave field inhomogeneities. The calculated Rabi frequency will, however, be proportional to the amplitude of the transition. Therefore we have calculated the Rabi frequency for N-photon transitions with various microwave field strengths. The results are shown in Fig. 10. Each solid circle represents an N-photon transition (N is plotted on the horizontal axis) for a particular microwave field strength (plotted on the vertical axis). The diameter of a circle is proportional to the calculated Rabi frequency. A transition is not shown if its calculated Rabi frequency is below the threshold for observation, given our

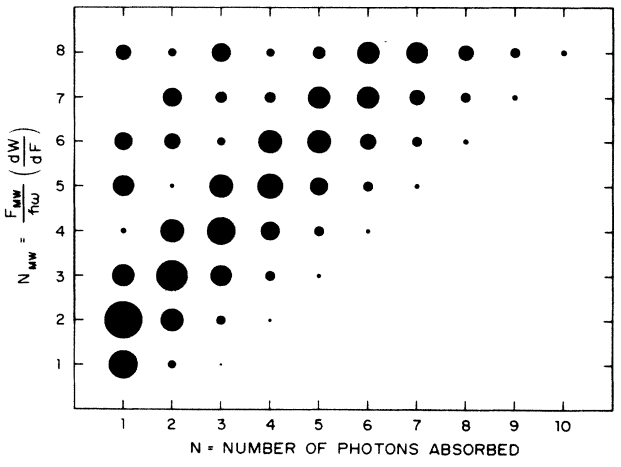

FIG. 10. Transition strengths calculated by numerical integration for N-photon transitions at various microwave fields. The diameter of a circle is proportional to the Rabi frequency of the calculated resonance. The microwave field is expressed as an equivalent number of photons N_{MW}. Note that the transition strengths are approximately constant along lines for which $dN_{MW}/dN = 1$, and are appreciable for $N - N_{MW} \leq 2$ (the two-photon offset).

detection sensitivity. The number N of photons absorbed is proportional to the static field relative to the crossing field and the microwave field is expressed as an equivalent number of photons N_{MW} (that is, proportional to the Stark shift dW/dF). Therefore the peak electric field, static plus microwave, exactly reaches the crossing field when $N_{MW} = N$. The resonance shown in Figs. 8 and 9 has $N_{MW} = N = 6$.

Figure 10 clearly shows that the transition probabilities are approximately constant along lines for which $dN_{MW}/dN = 1$. More specifically, the transition probabilities fall off sharply when $N > N_{MW}$. This is consistent with the Landau-Zener picture, which predicts that the transitions occur with appreciable probability when the total electric field reaches the crossing. The calculated threshold for observation of a particular transition does, however, exhibit the two-photon offset which was observed experimentally, as shown in Fig. 6. From the Landau-Zener point of view this effect is superficially surprising since transitions are observed even when the electric field does not reach the crossing. In this case, however, the transition probabilities are small but not zero since the coupling between the levels, although small, is not zero away from the crossing.

The Floquet, or dressed-atom, approach to this problem was first used by Autler and Townes[16] and it provides an alternative, perhaps more useful, way of approaching the multiphoton transitions. It is useful to first consider the problem of an atom in a combined static, F_s, and microwave, $F_{MW}\cos\omega t$, field in simple quasistatic terms. As level $|2\rangle$ has no Stark shift it is affected by neither the static nor microwave field. Level $|1\rangle$, on the other hand, has an average energy $W_1 - kF_s$ which is modulated by $\pm kF_{MW}$ at frequency $\omega/2\pi$. Thus the energy is not a constant. Stated another way the interval between the states $|1\rangle$ and $|2\rangle$ is frequency modulated at frequency $\omega/2\pi$. Just as for an FM radio signal, if the modulated frequency is Fourier analyzed it is found to consist of a carrier at $(W_1 - kF_s - W_2)/h$ with sidebands displaced by integral multiples of $\omega/2\pi$. Thus, as shown by Autler and Townes, the coefficient of $|1\rangle$ in the wave function of Eq. (1) in a field $F = F_s + F_{MW}\cos\omega t$ is given by

$$T_1(t) = e^{-it(W_1 - kF_s)/\hbar} \sum_{n=-\infty}^{\infty} J_n(kF_{MW}/\hbar\omega) e^{-in\omega t}, \quad (4)$$

where J_n is the Bessel function of order n. That is, the spatial wave function is unchanged, but there is no longer a single energy but an infinite number of them, at intervals of ω. We shall refer to the states at the new energies as sideband states in analogy with FM radio. At this point it is worth noting a few points about the Bessel function $J_n(x)$. For the large arguments relevant to the multiphoton processes of interest, the values of $J_n(x)$ are of comparable magnitude out to $x = n$, beyond which point the amplitudes fall by a factor of 10 in two sidebands.[19] Thus further sidebands have negligible amplitude and may be neglected. Thus the sidebands cover the energy range $\pm kF_{MW}$, as might be expected. In addition,

the energies of the sideband states have the same dependence on static field as does state $|1\rangle$.

The most convenient form of the solution to the problem at hand was worked out by Shirley.[17] A Floquet matrix, analogous to the usual Hamiltonian matrix, is diagonalized.[20] For our case the matrix is given by

$$\begin{pmatrix}
W_1-2\omega & b & \alpha & & & & & & & & \\
b & W_2-2\omega & 0 & & & & & & & & \\
\alpha & 0 & W_1-\omega & b & \alpha & & & & & & \\
 & & b & W_2-\omega & 0 & & & & & & \\
 & & \alpha & 0 & W_1 & b & \alpha & & & & \\
 & & & & b & W_2 & 0 & & & & \\
 & & & & \alpha & 0 & W_1+\omega & b & \alpha & & \\
 & & & & & & b & W_2+\omega & 0 & & \\
 & & & & & & \alpha & 0 & W_1+2\omega & b & \\
 & & & & & & & & b & W_2+2\omega &
\end{pmatrix} \tag{5}$$

where $\alpha = kF_{\mathrm{MW}}/2$. The blank entries are all zero. The matrix has several features which are worth noting. First, the diagonal energy levels occur in pairs, corresponding to the energies of states $|1\rangle$ and $|2\rangle$, plus or minus an integer number of photons. These states are coupled by the off-diagonal, field-independent coupling matrix element b. The sets of energy levels differing in energy by one photon are coupled by the microwave field through state $|1\rangle$ only. Notice also that the matrix is infinite, to account for all possible sidebands. To obtain reasonably accurate results, however, it is only necessary to include enough sidebands to ensure that all with appreciable amplitude are included. From our previous discussion of the Bessel function representation of level 1 we know that the number of sidebands required is approximately $N = (kF_{\mathrm{MW}}/\hbar\omega) + 2$.

When the matrix of Eq. (5) is diagonalized for fixed values of static and microwave fields it leads to energies as shown in Fig. 11, in which we have shown the carriers and sidebands as solid and dashed lines, respectively. Note that the sidebands tune along with the carrier. Note also that in addition to the avoided crossing of Fig. 8 (for which $F_{\mathrm{MW}}=0$), there are avoided crossings of the sideband states as well. As has been shown by Shirley,[17] the magnitudes of these avoided crossings at a particular static field are equal to the Rabi frequency for the multiphoton transition of interest. Thus by simply computing the eigenvalues of the Floquet matrix of Eq. (5) we are able to determine the transition rates. It is interesting to note that it is possible to observe experimentally the equivalence between multiphoton transitions and avoided level crossings of dressed atomic states. Specifically, we have detected the microwave multiphoton resonances as anticrossings between the $(n+2)s$ state and sidebands of the $(n,3)$ states by monitoring the population transferred to the $(n+2)p$ state by 300-K blackbody radiation. The blackbody-radiation transfer mechanism is discussed in Refs. 13 and 21.

Before presenting the results of the numerical diagonalization of the Floquet matrix, it is first useful to suggest a method for determining approximate solutions. As shown by Eq. (4), level 1 does not have a unique energy but is composed of a carrier and sidebands. To estimate the Rabi frequency of the coupling of one of these levels with level 2 we only need to calculate the matrix element

$$\langle 2 | V | 1_n \rangle = \langle 2 | V | 1 \rangle J_n(kF_{\mathrm{MW}}/\hbar\omega) , \tag{6}$$

where $|1_n\rangle$ represents the nth sideband state. This immediately implies that the total field must approach the level crossing.

This approach also allows us to generalize the case shown in Fig. 8 to the one in which both states have Stark shifts. In this case the matrix element between the mth sideband of level 2 and the nth sideband of level 1 is

$$\langle 2_m | V | 1_n \rangle = \langle 2 | V | 1 \rangle J_m(k_2 F_{\mathrm{MW}}/\hbar\omega) J_n(k_1 F_{\mathrm{MW}}/\hbar\omega) . \tag{7}$$

Similarly the coupling for the j-photon resonance, for which $|1\rangle$ lies $j\omega$ above $|2\rangle$, is a coherent addition of the amplitudes of several interacting sets of sidebands

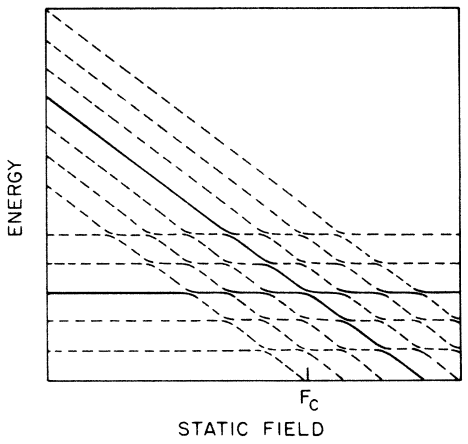

FIG. 11. Carrier and sideband energies, shown as solid and dashed lines, respectively. Note that the sideband levels, in addition to the carriers, undergo avoided crossings.

$$\langle 2 \mid V \mid 1 \rangle_k = \langle 2 \mid V \mid 1 \rangle \sum_{m=-\infty}^{\infty} J_{j-m}(k_2 F_{\mathrm{MW}}/\hbar\omega) \times J_m(k_1 F_{\mathrm{MW}}/\hbar\omega) \ . \quad (8)$$

The sum collapses to a single Bessel function,[19] and therefore

$$\langle 2 \mid V \mid 1 \rangle_k = \langle 2 \mid V \mid 1 \rangle J_k[(k_1 - k_2)F_{\mathrm{MW}}/\hbar\omega] \ . \quad (9)$$

Thus the conclusion derived from Fig. 8, in which only one state has a Stark shift, applies equally well to the case in which both states have Stark shifts. In the latter case it is only the differential Stark shift that is important.

We can now compare the Landau-Zener (field point of view) calculations with the results of the Floquet (photon point of view) matrix diagonalization. We wish to plot these results in such a way that they may be directly compared to the experimental results shown in Fig. 6, where the microwave field required to observe a particular multiphoton transition is plotted versus the number of photons absorbed. First we must determine the smallest observable Rabi frequency. The microwave pulse is on for 1 μs, but we are only able to observe linewidths as small as 1 GHz due to electric field inhomogeneity, implying a 1-ns coherence time. There are 10^3 coherence times in our 1-μs microwave pulse and we add their transition probabilities, which must be $\sim 10^{-3}$ to produce saturation. This occurs for a Rabi frequency of 30 MHz. Therefore we have chosen 30 MHz as the saturation Rabi frequency. The Landau-Zener and Floquet calculations provide the Rabi frequency for a given number of photons absorbed at a particular value of the microwave field. We can therefore determine the number of photons absorbed, for a given microwave field, at the 30-MHz saturation Rabi frequency. The Landau-Zener, Floquet, and experimental results are all shown in Fig. 12. The number of photons absorbed is expressed in frequency units so that the experimental results for both 9.278 and 10.353 GHz photons can be shown together. The simple Bessel-function expansion of Eq. (9) gives essentially the same results as the Landau-Zener and Floquet calculations shown in Fig. 12. This is not surprising since the photon energy is significantly larger than the avoided-crossing energy. As shown, the calculations based on the simple two-level model indicate less energy absorption than actually observed. This is not surprising in light of the interactions we have omitted from the model. What is important is that this simple model gives a clear picture of all the phenomena observed and is quantitatively correct to $\sim 30\%$.

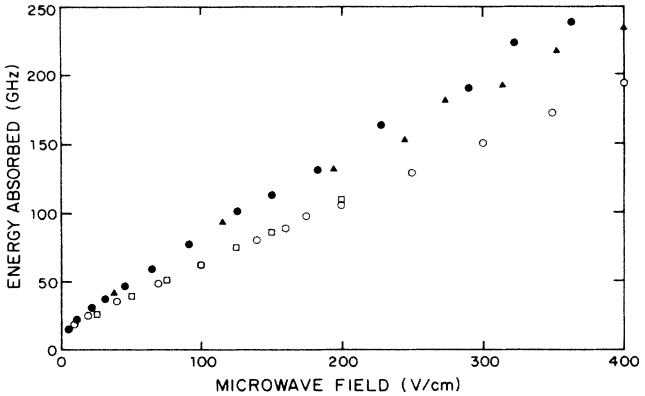

FIG. 12. Total energy (number of photons times photon energy) absorbed vs microwave field. The solid triangles indicate the 9.278-GHz data; solid circles, the 10.353-GHz data; open squares, Landau-Zener calculations; open circles, two-level Floquet calculations.

D. Dynamic Stark shifts

We have pointed out that the observed transitions from the $(n+2)s$ to the $(n,3)$ state (shown in Fig. 5 for $n=17$) are evenly spaced with respect to the static field. The spacing is only approximately uniform, however, and the deviation from uniformity is due at least in part to the deviations from linearity of the Stark shifts of the levels involved. The resonance fields can be predicted if the energies of the $(n+2)s$ and $(n,3)$ states are known as a function of the static electric field. We have chosen to calculate the energy levels by numerically diagonalizing[20] the energy matrix, using as the Hamiltonian

$$H = H_0 + F_s z \ , \quad (10)$$

where H_0 is the atomic Hamiltonian in the absence of electric fields and F_s is the static electric field which is assumed to lie along the z axis. The matrix elements of H are calculated in the n,l basis, for which H_0 is diagonal. The calculation is made tractable by including in the basis only those states which have energies in the neighborhood of the $(n+2)s$ and $(n,3)$ states. The zero-field atomic energies are known from spectroscopic measurements.[22,23] The radial matrix elements of z are found by numerically integrating the Coulomb radial equation.[20] This technique, while not the most elegant theoretically, has been found to give very accurate results for the static Stark shift.

When the resonance fields are calculated in this way, however, they differ from the observed resonance fields in a systematic way. The deviations are shown in Fig. 13 for transitions from the $(n+2)s$ state for n in the range 16–19. The shift, expressed as an energy, is plotted versus the square of the microwave electric field. The shift is evidently proportional to the square of the microwave field for a given n and therefore represents a dynamic polarizability, i.e., an ac Stark shift. The observed resonance fields are larger than the calculated fields, implying that the dynamic Stark shift causes the s state and the manifold state to repel. It is apparent from Fig. 13 that the dynamic polarizability increases regularly with n. Therefore it is reasonable to fit the observed dynamic polarizability α to a power law

$$\alpha = An^p \ . \quad (11)$$

A least-squares fit to Eq. (11) of the data in Fig. 13 gives $A = 2(2) \times 10^{-12}$ GHz(V/cm)^2 and $p = 5.9(8)$. The determination of the exponent p is reasonably good but

the fit gives very little information on the coefficient A. The fit parameters are used to plot the straight lines in Fig. 13.

It is interesting to compare the fit exponent with the result that we expect from simple theoretical arguments. Since the shift is quadratic in the field it can be calculated in second-order perturbation theory. Therefore the shift is expected to be a product of two dipole moments, with an energy denominator. Rydberg dipole moments are proportional to n^2, while energy intervals, which substantially exceed the microwave frequency, vary as $1/n^3$. Therefore the dynamic polarizability is expected to be proportional to n^7, which is in reasonable agreement with the exponent fit from the data.

E. Connection with microwave ionization

The appearance of a resonance in the microwave threshold spectrum discussed in Sec. III A is not surprising in light of the large magnitudes of the dynamic Stark shifts shown in Fig. 13. For 19s the observed shift is as much as half the photon energy. The appearance of a resonance is governed by several factors. These factors combine to produce an observed resonance for 19s, shown in Fig. 4, but not for 18s. The most fundamental of these factors is the energy separation of the $(n+2)s$ state and the n manifold when no fields are present. For the manifold energy we use the hydrogenic energy $-1/2n^2$, adjusted for the potassium nuclear mass. In Table II this separation is given for n in the range 16–21. The separation is expressed in units of the 9.278-GHz photon energy. The fractional part of this number determines the amount of dynamic Stark shift required to meet the resonance condition. We have already pointed out that the dynamic Stark shift repels the s state from the manifold. Therefore the resonance in the microwave spectrum corresponds to an absorption of N photons, where $N-1$ is the integer part of the zero-field separation shown in Table II. Given the zero-field separation, the dynamic polarizability, also shown in Table II, determines the field at which the resonance will appear. The calculated microwave resonance fields are given in the last column of Table II.

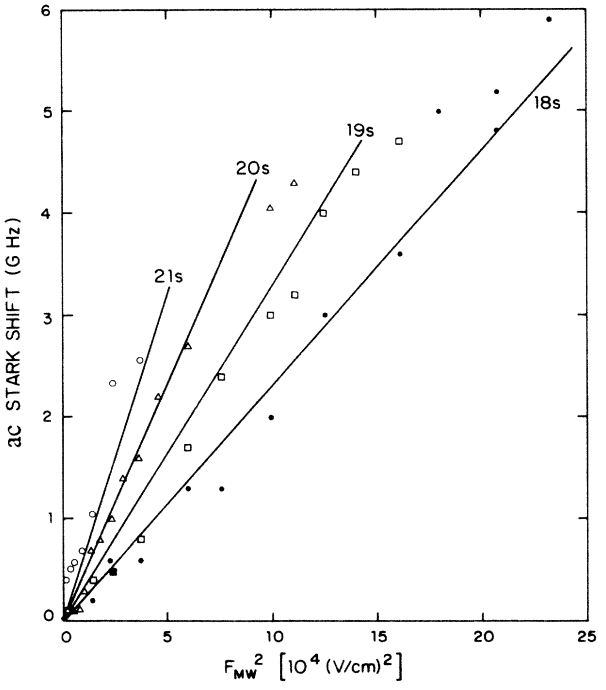

FIG. 13. Observed dynamic Stark shifts for multiphoton transitions from the $(n+2)s$ state to the $(n,3)$ manifold state. The data points represent the deviations of the observed resonances from those calculated using Eq. (10). Solid circles indicate $n=16$; squares, $n=17$; triangles, $n=18$; open circles, $n=19$. The lines are a least-squares fit of the data to the power-law equation (11).

The calculated resonance fields indicate potential resonances, which may or may not be observable, depending on the transition probabilities. A resonance will be observed only when the microwave field is within a limited range just below the s-state crossing field (shown in the last column of Table I). Roughly speaking, the two-photon offset shown in Fig. 6 determines this range. If the microwave field is too small the threshold condition of Fig. 6 will not be met and the resonance will be too weak to observe. If the microwave field is too large the resonance will not be resolved from the smooth threshold in the microwave spectrum. With this point in mind it is interesting to consider the origin of the smooth threshold. When a particular multiphoton transition is just above the observation threshold, for example, the leftmost peaks in each of the traces of Fig. 5, the resonance is narrow and well resolved from neighboring resonances. When the microwave field is increased, the strongest transitions broaden due to saturation and weaker transitions become observable. Thus the resonances representing transitions to the various manifold levels tend to blend together. This effect is most pronounced at zero static field, where the transition probabilities to the various manifold states are more uniform. It is this effect which gives the resonance in Fig. 4 its broad character. The blending process is accelerated by the quadratic nature of the dynamic Stark shift, which brings successive multiphoton transitions into resonance more rapidly. Therefore, at most, one resonance is observed before the smooth threshold is reached.

The observed threshold and resonance fields for the mi-

TABLE II. Calculated $F_s=0$ resonance fields.

$(n+2)s$ state	Number of 9.278-GHz photons separating $(n+2)s$ and $(n,3)$ states	Dynamic polarizability of $(n+2)s$ state [GHz/(V/cm)^2]	Calculated $F_s=0$ resonance field (V/cm)
18s	31.84	1.59×10^{-5}	306
19s	26.51	2.37×10^{-5}	438
20s	22.30	3.42×10^{-5}	436
21s	18.95	4.86×10^{-5}	98
22s	16.23	6.84×10^{-5}	323
23s	14.01	9.44×10^{-5}	312

crowave spectra are given in Table I. A resonance is resolved from the smooth threshold only for 19s, where the resonance corresponds to the 27-photon transition. The stated resonance field refers to the center of the resonance, while the tabulated threshold fields refer to the half maximum of the saturated signal. The observed threshold fields are generally somewhat above the s-state crossing fields, i.e., they generally increase monotonically as n decreases. The deviations from this behavior are explained by the calculated resonance fields. The most striking example of this effect is 20s, where the low value for the smooth threshold is explained by the calculated 23-photon resonance at 436 V/cm. In Sec. IV we will expand on the simple picture provided by Tables I and II by calculating in detail the energy-level structure as a function of the microwave field strength.

IV. FLOQUET CALCULATIONS

In Sec. III D the dynamic Stark shifts of the multiphoton transitions were determined by comparing the observed resonances with calculations based on Eq. (10). The shifts arose because the Hamiltonian of Eq. (10) did not include the microwave electric field. We can expect to account for the dynamic shifts if we use $F(t)$ from Eq. (2) for the electric field in place of F_s in the Hamiltonian of Eq. (10). Before doing this, however, it is instructive to consider the problem in the adiabatic approximation. In this approximation, which applies when the microwave frequency ω is low compared to the atomic energy separations, the variation of the field is treated quasistatically.[24] It is reasonable to expect the quasistatic description to apply since the s state is not coupled strongly to the linear Stark manifold, as can be seen in Fig. 1. In the quasistatic approximation, then, the energy of a level is given by the time-average

$$\langle E \rangle = \frac{1}{T} \int_0^T E(t) dt \ , \tag{12}$$

where $T = 2\pi/\omega$, i.e., the average is taken over a complete cycle of the microwaves. In general the energy of a particular level can be written approximately as

$$E(t) = AF(t) + BF^2(t) \ . \tag{13}$$

For the s state the Stark shift is approximately quadratic and $A \sim 0$. The manifold levels have approximately linear Stark shifts and $B \sim 0$. Using Eqs. (2), (12), and (13), the quasistatic energy is

$$\langle E \rangle = AF_s + BF_s^2 + \tfrac{1}{2} BF_{\mathrm{MW}}^2 \ . \tag{14}$$

The first two terms are just the linear and quadratic static Stark shifts while the third term is the dynamic Stark shift. Equation (14) therefore shows that, in the adiabatic approximation, levels with a quadratic static Stark shift also have a quadratic dynamic Stark shift (and that the dynamic polarizability is half the static polarizability), while levels with a linear static Stark shift have no dynamic Stark shift. The dynamic polarizabilities can therefore be found, in the adiabatic approximation, by diagonalizing the static Hamiltonian of Eq. (10). The results are given in the third column of Table II.

We will now calculate the dynamic Stark shifts without making the adiabatic approximation. We apply the numerical diagonalization method to the Hamiltonian of Eq. (10) as before, except that $F(t)$ from Eq. (2) will be used in place of F_s in Eq. (10). The application of the diagonalization method is complicated by the time dependence of the field. We will follow Autler and Townes[16] in applying the time-dependent Schrödinger equation, expanding in terms of Floquet (i.e., sideband or dressed) states, and thereby eliminating the time dependence from the energy matrix. Autler and Townes considered the case of a two-level system with $F_s = 0$. We will extend their treatment to allow for many atomic levels, and in general nonzero F_s.

The wave function of the system can be expanded in the n,l basis,

$$|\psi\rangle = \sum_k T_k |k\rangle \ , \tag{15}$$

where the $|k\rangle$ are the basis functions and the T_k are the time-dependent amplitudes. The zero-field energies ω_k are given by

$$H_0 |k\rangle = \omega_k |k\rangle \ , \tag{16}$$

and are known from spectroscopic measurements.[22,23] When Eq. (15) is substituted into the time-dependent Schrödinger equation, and the result is multiplied by $\langle j|$, we obtain

$$\omega_j T_j + F(t) \sum_k T_k \langle j|z|k\rangle = i\dot{T}_j \ , \tag{17}$$

where Eqs. (10) [with $F(t)$ substituted for F_s] and (16) have been used. At this point we make use of Floquet's theorem, which states that the solution of a differential equation with periodic coefficients can be written in the form

$$T_k = e^{-i\lambda t} \sum_{n=-\infty}^{+\infty} A_{nk} e^{-in\omega t} \ . \tag{18}$$

This expansion shows that the microwave field produces an infinite number of sideband (Floquet) states, equally spaced at the microwave frequency ω, with amplitudes A_{nk}. When the Floquet expansion, Eq. (18), is substituted into Eq. (17), we get, after expressing $\cos\omega t$ as a sum of exponentials and equating terms with like exponents,

$$(\omega_j - n\omega) A_{nj} + \sum_k [\beta_s^{jk} A_{nk} + \beta_{\mathrm{MW}}^{jk} (A_{n+1,k} + A_{n-1,k})] = \lambda A_{nj} \ , \tag{19}$$

where the definitions

$$\beta_s^{jk} = F_s \langle j|z|k\rangle \ , \tag{20}$$

$$\beta_{\mathrm{MW}}^{jk} = \frac{F_{\mathrm{MW}}}{2} \langle j|z|k\rangle \tag{21}$$

have been made. The problem is now considerably simplified, since Eq. (19) is independent of time.

For the two-level system which Autler and Townes

considered, Eq. (19) represents two coupled equations. They found solutions by rewriting these equations in a continued fraction form. Shirley[17] found that the solution of the Autler-Townes problem was simplified by writing the coupled equations in matrix form. To extend this approach to the multilevel problem we cast Eq. (19) in matrix form, where the A_{nj} are the basis vectors, and find the eigenvalues by numerical diagonalization. We will write the matrix in block form, where the blocks are identified with the atomic state j and the elements of each block are identified with the Floquet state n. If we restrict our attention to only two atomic states a and b, the matrix is

$$\begin{bmatrix} W_a-\omega & 0 & 0 & \beta_s & \beta_{\mathrm{MW}} & 0 \\ 0 & W_a & 0 & \beta_{\mathrm{MW}} & \beta_s & \beta_{\mathrm{MW}} \\ 0 & 0 & W_a+\omega & 0 & \beta_{\mathrm{MW}} & \beta_s \\ \beta_s & \beta_{\mathrm{MW}} & 0 & W_b-\omega & 0 & 0 \\ \beta_{\mathrm{MW}} & \beta_s & \beta_{\mathrm{MW}} & 0 & W_b & 0 \\ 0 & \beta_{\mathrm{MW}} & \beta_s & 0 & 0 & W_b+\omega \end{bmatrix} . \tag{22}$$

Only one sideband has been shown in Eq. (22). That is, n has been restricted to the values -1, 0, and $+1$ for each atomic state, making each block a 3×3 submatrix. The diagonal blocks have only diagonal elements, since $\beta_s^{jk}=\beta_{\mathrm{MW}}^{jk}=0$ for $j=k$. The off-diagonal blocks are tridiagonal submatrices.

In general, the matrix represented by Eq. (19) is infinite with respect to both j and n. Therefore, in practice, the matrix must be truncated in order to find the eigenvalues by numerical diagonalization. The result of one such diagonalization calculation is shown in Fig. 14, where the $n=17$ manifold energies are plotted as a function of the microwave field F_{MW}, for 9.278-GHz photons. The $n=17$ manifold ($l>2$ states) together with the nearest $l\leq2$ states (19s, 19p, and 17d) have been used as the atomic basis set. For this calculation each atomic state has been allowed 20 sidebands (on each side of the carrier). The three groups of levels shown in Fig. 14 are the $n=-1$ sidebands, the carriers, and the $n=+1$ sidebands of the $n=17$ manifold, in order of increasing energy. With only 20 sidebands allowed, it is clear from the second column of Table II that the sidebands of the $l\leq2$ states do not overlap with each other or the $n=17$ manifold (for reference, the quantum defects are $\delta_s=2.18$, $\delta_p=1.71$, and $\delta_d=0.27$). In spite of this apparent deficiency, however, the carrier and sideband energies in Fig. 14 are self-consistent (that is, offset by the microwave frequency) for microwave fields up to 400 V/cm. Above this field truncation error causes the sidebands to diverge from the carrier levels, but the calculation is apparently valid up to approximately 500 V/cm.

The bold line in Fig. 14 is the 19s energy plus 27 times the 9.278-GHz photon energy. Therefore the intersection of this level with the $n=17$ manifold carrier near 500 V/cm corresponds to the resonance of Fig. 4. That is, the observed resonance in Fig. 4 represents the 27-photon transition shifted into resonance by the dynamic Stark shift.

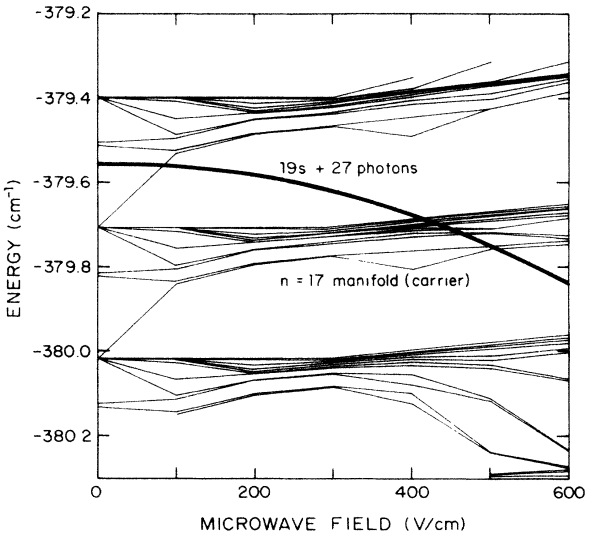

FIG. 14. Dynamic Stark structure calculated by numerical diagonalization of the Floquet matrix for 9.278-GHz photons. The $n=17$ manifold levels ($l>2$), plus their nearest sidebands (plus and minus one photon), are shown. The bold line is the 19s energy plus 27 times the 9.278-GHz photon energy. The intersection of the 19s plus 27-photon level with the $n=17$ manifold corresponds to the resonance of Fig. 4.

When Figs. 1 and 14 are compared it is clear that for the manifold levels the dynamic Stark effect is much smaller than the static Stark effect. On the other hand, the s state shown in Fig. 14 clearly has a quadratic dynamic Stark shift. These observations are in agreement with the quasistatic arguments as expressed by Eq. (14). Given this qualitative agreement, it is interesting to compare quantitatively the s-state dynamic polarizabilities obtained from the quasistatic model (the third column of Table II) with the diagonalization of the Floquet matrix. The agreement is surprisingly good, being better than 1% for all the states listed in Table II. It is also interesting to calculate the s-state dynamic polarizabilities using a variety of truncations of the (infinite) Floquet matrix. Specifically, we use as the basis set either the manifold plus one set of $l\leq2$ states or the manifold plus two sets of $l\leq2$ states, and for each choice of atomic basis set we use either 5, 10, or 20 sidebands. Remarkably, the resulting s-state dynamic polarizabilities are all within less than 1% of each other. Even more surprisingly, the results are unchanged when the manifold states are excluded from the matrix, and the basis consists only of s, p, and d states.

It is also interesting to calculate the dependence of the dynamic Stark shift of the s state on the static electric field. For values of the microwave field F_{MW} less than the crossing field F_c, the dynamic polarizabilities are found to be independent of the static field F_s (that is, in agreement within 1% with the values given in Table II).

Finally, we have determined the dependence of the calculated s-state dynamic polarizability on the principle

quantum number n. That is, we can fit the values from the third column of Table II to the power-law equation (11). This yields $p = 6.5(1)$ for the calculated polarizability, in agreement with the experimental result (Fig. 13 data) of $p = 5.9(8)$.

V. CONCLUSION

We have examined the connection between microwave ionization and microwave multiphoton transitions in Rydberg states of potassium. We have seen that these phenomena can be explained equally well with either the Landau-Zener model or the Floquet (dressed atom) picture. The multiphoton transitions are observed to have large dynamic Stark shifts which are in agreement with numerical calculations of the shifts. Resonances in the microwave ionization spectrum are seen to be multiphoton transitions which are shifted into resonance by the dynamic Stark shift. In contrast, the broad threshold observed in microwave ionization is due to many broadened and therefore unresolved multiphoton transitions.

ACKNOWLEDGMENTS

We thank Louis A. Bloomfield and Daniel J. Larson for helpful discussions. This work was supported by the U.S. Air Force Office of Scientific Research under Grant No. AFOSR-87-0007.

[1]T. W. Ducas, M. G. Littman, R. R. Freeman, and D. Kleppner, Phys. Rev. Lett. **35**, 366 (1975).

[2]T. F. Gallagher, L. M. Humphrey, W. E. Cooke, R. M. Hill, and S. A. Edelstein, Phys. Rev. A **16**, 1098 (1977).

[3]M. G. Littman, M. M. Kash, and D. Kleppner, Phys. Rev. Lett. **41**, 103 (1978).

[4]T. F. Gallagher and W. E. Cooke, Phys. Rev. A **19**, 694 (1979).

[5]T. H. Jeys, G. W. Foltz, K. A. Smith, E. J. Beiting, F. G. Kellert, F. B. Dunning, and R. F. Stebbings, Phys. Rev. Lett. **44**, 390 (1980).

[6]W. van de Water, D. R. Mariani, and P. M. Koch, Phys. Rev. A **30**, 2399 (1984).

[7]P. Pillet, W. W. Smith, R. Kachru, N. H. Tran, and T. F. Gallagher, Phys. Rev. Lett. **50**, 1042 (1983).

[8]D. R. Mariani, W. van der Water, P. M. Koch, and T. Bergeman, Phys. Rev. Lett. **50**, 1261 (1983).

[9]P. Pillet, H. B. van Linden van den Heuvell, W. W. Smith, R. Kachru, N. H. Tran, and T. F. Gallagher, Phys. Rev. A **30**, 280 (1984).

[10]J. R. Rubbmark, M. M. Kash, M. G. Littman, and D. Kleppner, Phys. Rev. A **23**, 3107 (1981).

[11]L. A. Bloomfield, R. C. Stoneman, and T. F. Gallagher, Phys. Rev. Lett. **57**, 2512 (1986).

[12]S. Ramo, J. R. Whinnery, and T. van Duzer, *Fields and Waves in Communication Electronics*, 2nd ed. (Wiley, New York, 1984).

[13]R. C. Stoneman, G. Janik and T. F. Gallagher, Phys. Rev. A **34**, 2952 (1986).

[14]L. D. Landau and E. M. Lifshitz, *Quantum Mechanics: Nonrelativistic Theory*, 3rd ed. (Pergamon, New York, 1977), pp. 342–351.

[15]C. Zener, Proc. R. Soc. London, Ser. A **137**, 696 (1932).

[16]S. H. Autler and C. H. Townes, Phys. Rev. **100**, 703 (1955).

[17]J. H. Shirley, Phys. Rev. **138**, B979 (1965).

[18]N. F. Ramsey, *Molecular Beams* (Oxford, New York, 1956), pp. 118–120.

[19]*Handbook of Mathematical Functions*, Nat. Bur. Stand. Appl. Math. Ser. No. 55, edited by M. Abramowitz and I. A. Stegun (U.S. GPO, Washington, D.C., 1964).

[20]M. L. Zimmerman, M. G. Littman, M. M. Kash, and K. Kleppner, Phys. Rev. A **20**, 2251 (1979).

[21]R. C. Stoneman and T. F. Gallagher, Phys. Rev. Lett. **55**, 2567 (1985).

[22]P. Risberg, Ark. Fys. **10**, 583 (1956).

[23]D. C. Thompson, M. S. O'Sullivan, B. P. Stoicheff, and Gen-Xing Xu, Can. J. Phys. **61**, 949 (1983).

[24]P. Pillet, R. Kachru, N. H. Tran, W. W. Smith, and T. F. Gallagher, Phys. Rev. A **36**, 1132 (1987).